



ENGINEERING SCIENCES

Optimization of the adsorption and desorption processes of nickel octaethylporphyrin in carbon-based adsorbents

GABRIELA C. CAETANO, LAIANE A. DE ANDRADE, PAULO ROBERTO MARTINS & INDIANARA C. OSTROSKI

Abstract: Despite being little explored for petroporphyrins recovery from oils and bituminous shales, adsorption and desorption processes can be feasible alternatives to obtain a similar synthetic material, and to characterize their original organic materials. Experimental designs were used to analyze the effects of qualitative (e.g., type of adsorbent, solvent, and diluent) and quantitative (e.g., temperature and solid/liquid ratio) variables on the adsorptive and desorptive performance regarding nickel octaethylporphyrin (Ni-OEP) removal using carbon-based adsorbents. The evaluation variables, adsorption capacity (q_e) and desorption percentage ($\%_{desorption}$) were optimized by means of the Differential Evolution algorithm. The most efficient adsorbent for removing/recovery Ni-OEP was activated-carbon coconut shell, in which dispersive π - π type and acid-base interactions were likely formed. The highest values of q_e and $\%_{desorption}$ were obtained using toluene as solvent, chloroform as diluent, 293 K as temperature, and 0.5 mg.mL⁻¹ as solid/liquid ratio for adsorption, and a higher temperature (323 K) and lower solid/liquid ratio (0.2 mg.mL⁻¹) for desorption. The optimization process resulted in q_e of 6.91 mg.g⁻¹ and $\%_{desorption}$ of 35.2%. In the adsorption-desorption cycles, approximately 77% of the adsorbed porphyrins were recovered. The results demonstrated the potential of carbon-based materials as adsorbent materials for obtaining porphyrin compounds from oils and bituminous shales.

Key words: adsorption separation, biomarker, desorption recovery, multiobjective problem optimization, petroporphyrin.

INTRODUCTION

The availability reduction of light and medium oils sources, and the continuous increase in energy demand worldwide have made the exploration and processing of heavy oils a challenge for the oil industry (Demirbas et al. 2016, Silva et al. 2017). The high levels of heteroatoms and contaminants in non-conventional oils hampers their refining (Rytting et al. 2019). Thus, the identification of regions that potentially produce lighter oils can be an interesting alternative. Regarding the process of assessing the quality

of oil sources, the biomarkers distribution is an important factor to be considered (Affouri & Sahraoui 2017).

Porphyrins are an important class of biomarkers used to investigate the degree of oil maturity (Yang et al. 2018). Porphyrin structures are tetrapyrrolic, heterogeneous and aromatics, the result of the transformation of primary chloropigments which occurs during the processes of oil formation and maturation (Ramírez-Pradilla et al. 2019, Zhang et al. 2019). The porphyrins are present in the most polar fractions of petroleum, asphaltenes, and resins

(Mousavi et al. 2019). In bituminous shales, the porphyrins are commonly found in oil and mainly distributed in etioporphyrins (ETIO), deoxyphylloerythroetioporphyrins (DPEP), and rhodoporphyrins (RHODO) (Dechaine & Gray 2010). Actually, the most abundant metalloporphyrins in oil are nickel and oxovanadium porphyrins (Liu et al. 2015a, Zhao et al. 2015).

Despite being found in the form of trace elements in oil (Poirier et al. 2016, Sama et al. 2018, Sugiyama & Williams-Jones 2018), these compounds are capable of altering the oil physical-chemical properties (Silva et al. 2017), promoting corrosion of pipes and equipment (Wang et al. 2016). They also poison the catalysts employed (Etim et al. 2016, 2019), harming the quality and yield of refining products (Sorokina et al. 2010), hence contributing to environmental pollution (Sama et al. 2018).

Provided the damages caused to the oil processing, the removal and recognition of the porphyrinic species, and others nitrogen and sulfur contaminants (Saleh 2020), from their origin oil is highly recommended. Qualitative and quantitative analyses of petroporphyrins are necessary to identify the oil properties as well as the potential damage to the refining. Meanwhile, their recovery allows the application of their optical and electronic properties (Gottfried 2015, Hips & Mazur 2018, Jurow et al. 2010, Kuzmin et al. 2018, Lee et al. 2017). The use of synthetic porphyrins and metalloporphyrins is observed in areas related to surface science (Hips & Mazur 2018), such as catalysis (Kuzmin et al. 2018), and in mechanisms involving energy transfer, due to their photoelectronic properties, being potential components of electronic devices, such as wires and diodes (Jurow et al. 2010). Moreover, the photodynamic activity of sedimentary porphyrins, such as oxovanadium etioporphyrin, has already been observed (Ribeiro et al. 2005).

Among the porphyrins separation and isolation methods currently employed, the extractive and chromatographic methods are predominant (Kumolo et al. 2019, Liu et al. 2015b, Mironov et al. 2017, 2018a, b, Rytting et al. 2018, Woltering et al. 2016, Yakubov et al. 2017). Although the high efficiency of these methods, they are associated with some disadvantages such as the high consumption of solvents and inputs (Li et al. 2020), and the limited treatment and supply (Zhang et al. 2019). The use of adsorption processes can be a more sustainable alternative, although it has been little explored for this purpose (Chen et al. 2013, 2017, 2018). Chen et al. (2013, 2017) evaluated the possible interaction mechanisms between porphyrins and asphaltenic compounds using kinetic, equilibrium and thermodynamic adsorption studies of nickel (Ni-OEP) and oxovanadium octaethylporphyrins (VO-OEP) on asphaltene. Chen et al. (2018) analyzed the polyaromatic nuclei function of the adsorbents used by comparing the results obtained in previous studies (Chen et al. 2013, 2017), with the adsorption of the same porphyrins onto graphene. No study has suggested the recovery of petroporphyrin compounds.

Extensive use of carbon-based materials as adsorbents is observed in the removal of several pollutants (Bin-Dahman & Saleh 2020, Saleh et al. 2020). However, its use for the adsorption of petroporphyrins from oil is still scarce. The related studies focused on discussing the properties and mechanism of self-assembled structures formation of metalloporphyrins adsorbed onto graphitic materials (Gruden-Pavlović et al. 2007, Hips & Mazur 2018, Ogunrinde et al. 2006).

However, their use for the removal of nitrogenous components is recurrent in the literature (Carvalho et al. 2020, Feng et al. 2015, Ferreira et al. 2019, Han et al. 2015, Wen et al. 2017). The performance of these materials is directly

associated with their surface chemistry and pore structure (Wen et al. 2017). The presence of acidic functional groups in their structure may favor the adsorption of basic nitrogen regions, such as those available in the porphyrinic molecule (Lee et al. 2017), forming acid-base interactions (Han et al. 2015). Although the presence of functional groups on the adsorbent surface can be a facilitator for the adsorptive process, the recovery of the adsorbate through the subsequent desorption process can be difficult (Prado et al. 2016). Some works revealed the high efficiency of toluene and chloroform in the regeneration of adsorbent materials used in the removal of organic contaminants from liquid fuels (Almarri et al. 2009 Koriakin et al. 2010, Sano et al. 2004, Shah et al. 2017).

The knowledge of the physical-chemical and textural characteristics of the materials is not the only important factor for controlling the adsorptive and desorptive processes (Moskvin 2016). The study of the interactions between the operational parameters in the system's behavior is also a key factor to be considered. The statistical designs are widely used to optimize and model the experiments in the industrial sector since improvements in performance, reliability, capacity, and yield of processes were previously observed (Regti et al. 2017).

The recognized importance of porphyrin compounds in surface science applications increased the scientific interest and market value of these materials. The difficulty of separating petroporphyrin compounds and the possibility of using them as alternatives to their synthetic analogues also contribute to their high added value. The price of synthetic VO-OEP is around USD 2.72/mg, while the synthetic Ni-OEP reaches USD 4.35/mg (Sigma Aldrich 2021). The lack of studies regarding petroporphyrin recovery processes can be a limiting factor for the development of optimized operational

conditions. In this context, the present study aimed to evaluate the influence of experimental conditions, adsorbents' carbonic structure, solvent types, temperature, and solid/liquid ratio on the performance of Ni-OEP adsorption/desorption processes through experimental designs. The results obtained were quantified using the variables responses to adsorption capacity at equilibrium (q_e) and desorption percentage ($\%_{desorption}$), which were statistically treated and optimized.

MATERIALS AND METHODS

Materials

Nickel octaethylporphyrin (Ni-OEP: C₃₆H₄₄N₄Ni, 591.45 g.mol⁻¹, purity > 97%, Figure 1a), a structure similar to the nickel ethioporphyrin (Ni-ETIO, Figure 1b), was purchased from Sigma Aldrich. The adsorbent materials were used in the form of particles with a diameter of <150 μm. Granular coconut shell activated carbon (*Elaeis guineenses* - CSAC) was kindly donated by Bahiacarbon Agro-industrial Ltda. (Bahia Brazil). Graphite (G), in flakes format, was purchased from Sigma Aldrich, while graphite oxide (GO) was synthesized by means of the modified Hummers' method (Marcano et al. 2010). The solvents used were analytical: toluene (99.9%) from Bio-Grade, chloroform (99.8%) from Isofar, and dichloromethane (99.9%) from TEDIA High Purity Solvents.

The adsorption and desorption experiments were carried out in batch, under agitation in a rotary shaker (Ethik Technology, 430/RDB), at 120 rpm. The concentrations of porphyrin solutions were determined using an ultraviolet-visible spectrophotometer (BEL Photonics 1105). Residual solutions were analyzed in a spectrophotometer in triplicate values. The adsorbents were characterized by X-ray diffraction (XRD), nitrogen adsorption and

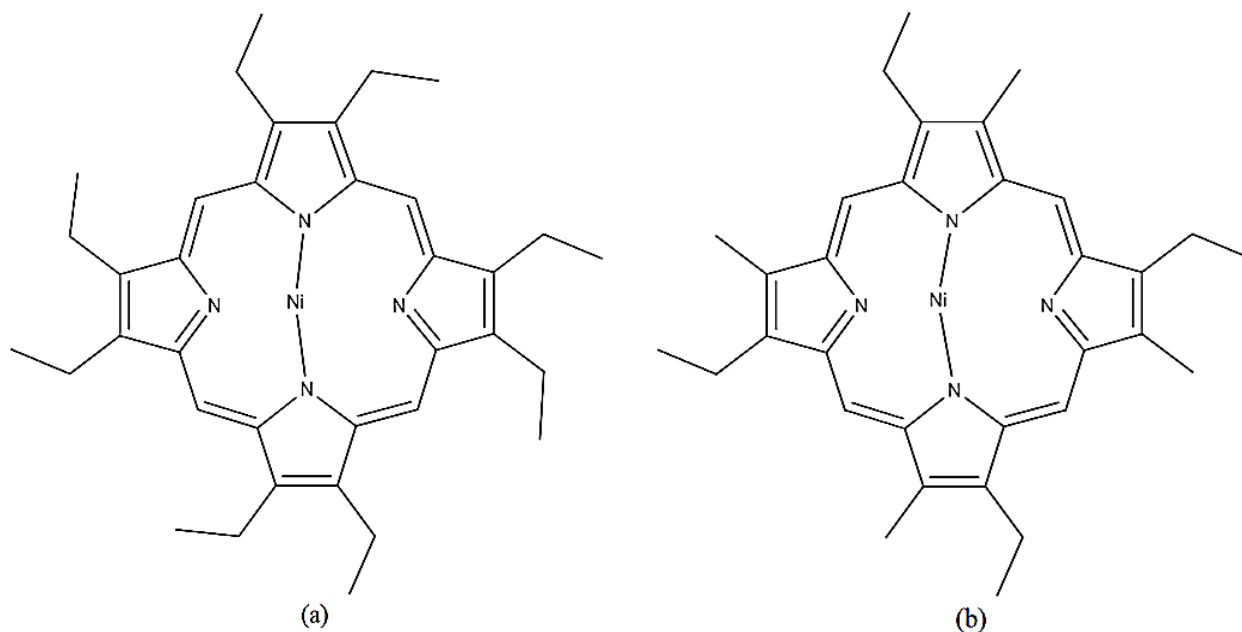


Figure 1. Structural formula of (a) nickel octaethylporphyrin (Ni-OEP) and (b) nickel ethioporphyrin (Ni-ETIO).

desorption (N_2) and infrared spectroscopy (IR). XRD analysis was performed on a Shimadzu DRX-6000 diffractometer with a copper source, at 40 kV and 20 mA. Measurements were performed in a 2θ range from 5 to 80 deg, with 0.02 deg/step. The adsorbents specific areas and porosity were analyzed through the adsorption and desorption of N_2 , at 77 K, using the ASAP 2020 Plus 1.03 (Micromeristic) equipment, in the relative pressure range (P/P_0) from 10^{-3} to 1. The specific area was determined by the Brunauer - Emmett - Teller (BET) multipoint technique (Brunauer et al. 1938). The total pore volume per total single point pore volume, ($P/P_0 = 0.98$), while the micropore volume was determined by the t-plot method (Lippens & De Boer 1965). The average pore diameter was determined by the Barrett-Joyner-Halenda (BJH) method (Barrett et al. 1951). The functional groups on the surface of the adsorbent materials were analyzed using MIR analysis, performed on a PerkinElmer spectrophotometer (model Spectrum 400), in a wavelength range from 4000 to 450 cm^{-1} .

Adsorbent selection

In order to evaluate the performance of CSAC, G and GO in the adsorption of nickel porphyrin, Ni-OEP solutions in toluene were subjected to initial adsorption tests, varying the adsorbent used. The experiments were carried out in batches, in which an initial porphyrin concentration of 8 $\mu g \cdot mL^{-1}$ was used, with 10 mL volumes and 5 mg adsorbent doses. The systems were kept under agitation (120 rpm) in a rotary shaker for 24 h at 298 K. The adsorption capacities at equilibrium (q_e) were calculated by Equation 1, which is given below:

$$q_e = (C_0 - C_e)VM \quad (1)$$

where C_0 is the initial solution concentration; C_e is the solution concentration at equilibrium; V is the solution volume; and M is the adsorbent mass.

The saturated adsorbents were subjected to subsequent desorption processes with chloroform in order to select the best adsorbent

for Ni-OEP adsorption and desorption. After adsorption, the saturated adsorbents were dried in an oven (353 K, 24 h) and underwent batch desorption tests. Doses of 1 mg were used, in contact with 5 mL of diluent, being kept under the same conditions of stirring (120 rpm), time (24 h) and temperature (298 K) as the adsorption tests. The desorption percentages ($\%_{desorption}$) were calculated by Equation 2, which is given below:

$$\%_{desorption} = q_{e,des}/q_e \times 100 \quad (2)$$

where q_e is the adsorption capacity at equilibrium (mg.g^{-1}); and $q_{e,des}$ is the desorption capacity at equilibrium (mg.g^{-1}), being calculated by Equation 3:

$$q_{e,des} = C_d V_{dil}/M_s \quad (3)$$

where C_d is the solution concentration at the end of the desorption; V_{dil} is the diluent volume; and M_s is the mass of the saturated adsorbent.

The highest values obtained for q_e and $\%_{desorption}$ were determinant to select the most efficient adsorbent for both adsorption and desorption of Ni-OEP, within the experimental conditions employed.

Experimental designs

Once the best adsorbent material was selected, the influence of solvent, diluent, temperature and solid/liquid ratio of adsorption and desorption on q_e and $\%_{desorption}$ was evaluated using experimental designs. Batch adsorption and desorption tests were performed under experimental conditions similar to those used in the initial tests. 10 mL of solutions with initial concentrations of $8 \mu\text{g.mL}^{-1}$ were subjected to the adsorption process for 24 h, under agitation at 120 rpm, changing the analyzed variables according to the experimental designs. While the volumes of diluent used in the desorption were 5 mL, they were also kept under agitation at 120 rpm for 24 h.

The results obtained were analyzed using statistical treatment. The regression equations were obtained as a function of the quantitative variables evaluated, and the conditions of temperature and solid/liquid ratio of both adsorption and desorption were optimized.

Qualitative experimental design

The effects of qualitative variables (solvent and diluent) on q_e and $\%_{desorption}$ were analyzed using a qualitative factorial design 2^2 . The levels of the variables evaluated are shown in Table I.

The results obtained in the qualitative

Table I. Levels of the variables evaluated in the qualitative experimental design.

Factor	Level	
	-1	+1
Solvent	Toluene	Chloroform
Diluent	Chloroform	Dichloromethane

tests, which the adsorption capacity in the equilibrium and the percentage of desorption were evaluated, allowed the elucidation of the performance of each solvent and diluents used in the adsorption and desorption processes, respectively.

Quantitative experimental design

The effects of quantitative variables, temperature, and solid/liquid ratio on q_e and $\%_{desorption}$ were analyzed using quantitative experimental designs.

First, the influence of temperature (T_{ads}) and solid/liquid ratio ($(S/L)_{ads}$) on the adsorption process performance was evaluated, being measured by the q_e value. An orthogonal central composite (CCOD) design was used, with 2 central points and 2^2 axial points (2.1.10). The levels used for the variables evaluated are shown in Table II.

Table II. Levels of the factors used in the study of the effect of the adsorption temperature and solid/liquid ratio on the adsorption of Ni-OEP in CSAC, using a CCOD 2.1.10 ($\alpha = 1.078$).

Factor	Code	Level				
		- α	-1	0	+1	+ α
T_{ads} (K)	x_1	294	295	313	331	332
$(S/L)_{ads}$ (mg.mL ⁻¹)	x_2	0.50	0.55	1.25	1.95	2.00

Table III. Levels of the factors used in the study of the effect of the adsorption and desorption temperature and solid/liquid ratio on the desorption of Ni-OEP in CSAC, using a CCOD 4.1.26 ($\alpha = 1.483$).

Factor	Code	Level				
		- α	-1	0	+1	+ α
T_{ads} (K)	x_1	294	300	313	326	332
$(S/L)_{ads}$ (mg.mL ⁻¹)	x_2	0.50	0.75	1.25	1.75	2.00
T_{des} (K)	x_3	293	298	308	318	323
$(S/L)_{des}$ (mg.mL ⁻¹)	x_4	0.20	0.25	0.35	0.45	0.50

The effects of adsorption (T_{ads}) and desorption (T_{des}) temperatures and adsorption ($(S/L)_{ads}$) and desorption ($(S/L)_{des}$) solid/liquid ratios on $\%_{desorption}$ were evaluated by means of CCOD, with 2 central points and 2³ axial points (4.1.26). The levels used for the variables evaluated are shown in Table III.

Optimization

The regression equations obtained for the variables evaluated were used in combination with the Differential Evolution algorithm (Storn & Price 1997), to determine the conditions of $T_{ads/des}$ and $(S/L)_{ads/des}$, which simultaneously maximize q_e and $\%_{desorption}$. Provided it is multiobjective optimization problem, the weighted sum method (Marler & Arora 2010) was used to obtain a single solution point. It was performed by applying weights to the response variables. This method was applied to an optimization code available in the MATLAB 2020 simulation program, similar to the methodology used by Silva et al. (2015). The optimization results obtained were evaluated to verify the consistency of the response surfaces

constructed for q_e and $\%_{desorption}$ variables. They were validated through new adsorption and desorption tests.

Adsorption-desorption cycles

Consecutive cycles of Ni-OEP adsorption and desorption were carried out in batches to evaluate the porphyrin recovery capacity and regeneration of the selected adsorbent after successive processes. The $q_{e/des}$ and $\%_{removal/desorption}$ were evaluated at each adsorption-desorption cycle. The experimental conditions used to concern temperature and solid/liquid ratio corresponded to those obtained by the optimization process.

RESULTS AND DISCUSSION

Adsorbent characterization

The diffraction patterns obtained for the adsorbent materials are shown in Figure 2. The GO formation was confirmed by the presence of a broad peak at $2\theta = 10.34^\circ$, corresponding to the

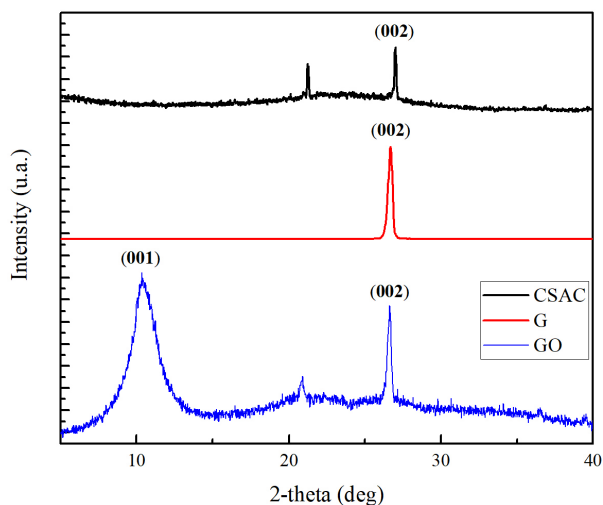


Figure 2. XRD patterns of (a) CSAC, (b) G and (c) GO materials, in a 2θ range from 5 to 80 deg.

plane (001) (Asgar et al. 2018). The characteristic peak of graphite at $2\theta \sim 26.55^\circ$, corresponding to the plane (002), are evidenced in the three materials spectra, suggesting the presence of residual graphitic material in the synthesized GO (Prado et al. 2016), and a basal carbonic structure akin to the graphite structure, with sp^2 hybridization carbons. The occurrence of other peak in the XRD pattern of the GO material at a smaller diffraction angle suggests the presence of layers with greater interplanar distances in the GO structure in comparison to graphite ($d_{002} = 0.335$ nm), in accordance with Bragg's Law (Khan et al. 2020). Greater interplanar distances may favor the formation of (multi)layers of adsorbed compounds and greater adsorption capacities, due to the possibility of reaching the adsorbate molecules (Kang et al. 2020).

The functional groups on the surface of the CSAC, G and GO materials were identified through the IR spectra, according to Zhao et al. 2019, as shown in Figure 3.

The constitution of the materials basic structure is revealed by the presence of bands at wavelengths close to 1632 cm^{-1} in the spectra, characteristics of $C=C$ stretches. The $C-C$

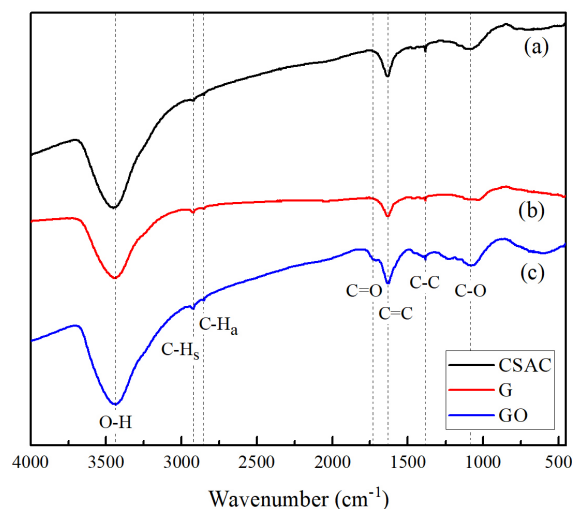


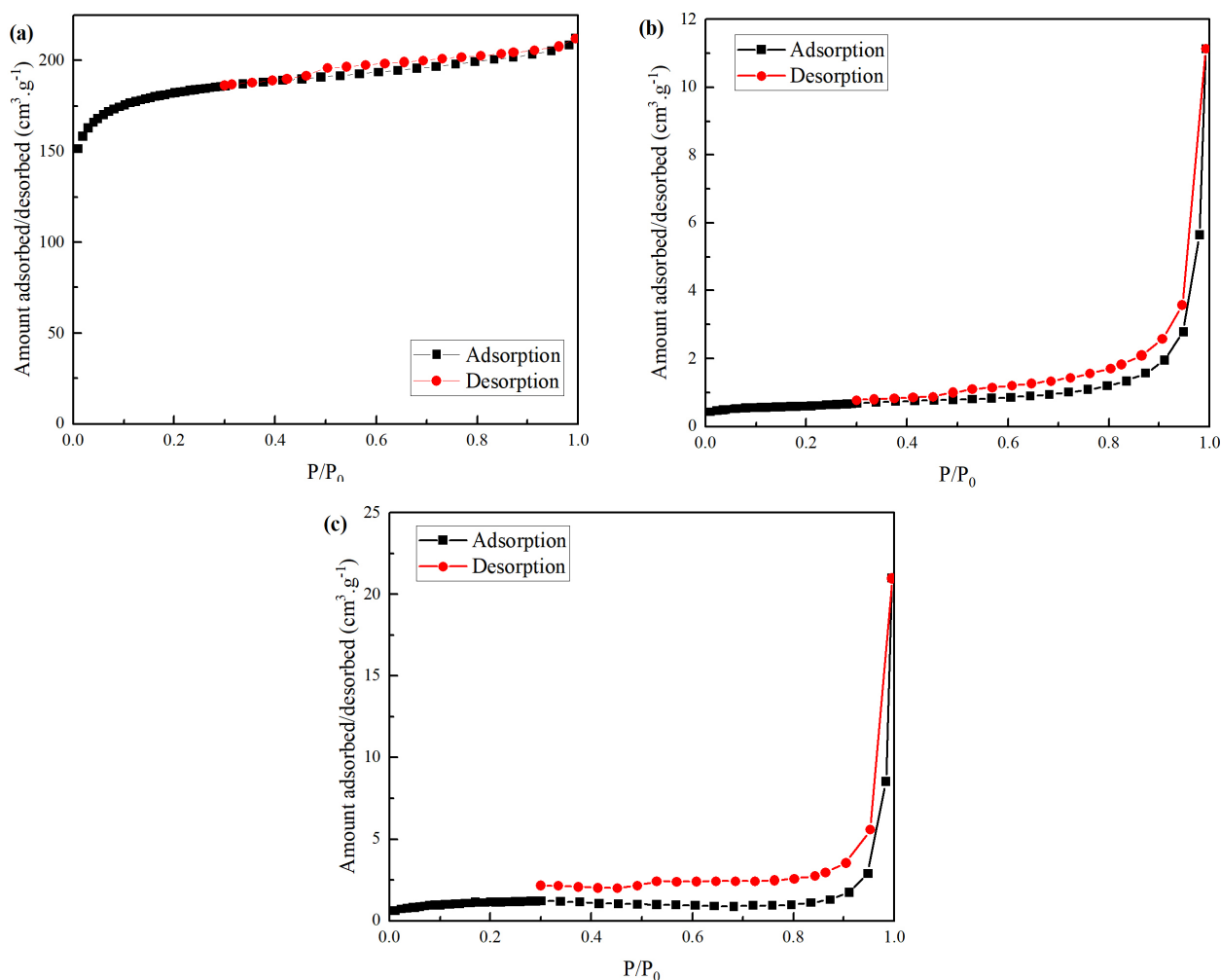
Figure 3. IR spectra of (a) CSAC, (b) G and (c) GO materials, in a wavelength range from 4000 to 450 cm^{-1} .

stretches, identified by bands at 1384 cm^{-1} , might be associated with the presence of branches in the carbonic skeleton, mainly in CSAC and GO materials. In these functionalized materials, bands close to 1090 cm^{-1} are also evident, characteristic of $C-O$ bonds. It suggests the presence of epoxy groups on their surfaces. Carbonyl groups ($C=O$), characteristic of the band close to 1725 cm^{-1} , may indicate the presence of carboxylic or aldehydic functional groups in the synthesized GO structure. The bands at 3445 cm^{-1} , common to the three materials evaluated, are characteristic of hydroxyl-type groups ($O-H$), indicating the likely presence of moisture or alcohols in the structures of the functionalized materials (CSAC and GO). The predominance of acidic functional groups on the surface of the GO is remarkable, as has already been observed (Channei et al. 2018). The peaks corresponding to the acid groups distributed on the surface of the GO are similar to those obtained by acid treatment of carbon-based materials (Saleh 2011). While basic and acidic functional groups can be found on the surface of other materials, with higher peak intensities of polar groups observed for CSAC.

Table IV. Specific area, volume of pores and micropores and average pore diameter of adsorbent materials, calculated by BET multipoint technique and BJH method, through N₂ adsorption/desorption.

Adsorbent	Total Pore Area (m ² .g ⁻¹)	Total Pore Volume (cm ³ .g ⁻¹)	Micropore Volume (cm ³ .g ⁻¹)	Pore diameter (nm)
CSAC	545.45	0.326	0.224	2.39
G	2.04	0.015	3.44x10 ⁻⁴	28.75
GO	3.68	0.025	4.97x10 ⁻⁴	27.51

Abbreviations: CSAC, coconut shell activated carbon; G, graphite; GO, graphite oxide.

**Figure 4.** N₂ adsorption/desorption isotherms at 77K and pore distribution curves, for (a) CSAC, (b) G and (c) GO.

The values obtained for specific area, total pore volume, micropore volume and average pore diameter are shown in Table IV, and the N₂ adsorption/desorption isotherms are

illustrated in Figure 4. Higher values of specific area, total volume of pores and micropores were observed for activated carbon in relation to graphical materials. Considering the

Table V. Comparison between the results of q_e and $\%_{desorption}$ obtained for different carbon-based materials in the adsorption and desorption tests, both with initial solution of $8 \mu\text{g}\cdot\text{L}^{-1}$, at 298K, under agitation of 120 rpm for 24 h.

Adsorbent	q_e ($\text{mg}\cdot\text{g}^{-1}$)	$\%_{desorption}$ (%)	Reference
CSAC	5.73 ± 0.10	30.9 ± 0.7	This work
G	1.45 ± 0.04	50.5 ± 0.8	This work
GO	1.91 ± 0.12	0	This work
Graphene	5.14	Unvalued	Chen et al. 2018
Asphaltene	4.45	Unvalued	Chen et al. 2017

Abbreviations: CSAC, coconut shell activated carbon; G, graphite; GO, graphite oxide.

parameters established by IUPAC (Thommes et al. 2015), as for the pore diameter, CSAC can be characterized as a predominantly microporous adsorbent. While G and GO have characteristics of nonporous materials, such as low values of total pore volume, micropore volume and total specific area, differently mesoporous graphite and graphite oxide (Channei et al. 2018). Low amounts of adsorbed N_2 (Figures 4b and 4c) are also indicative of the low presence of pores on the surface of graphitic materials.

In general, micropores are more favorable adsorption sites for the formation of adsorbate-adsorbent interactions (i.e., when the adsorbate molecule and adsorbent pore sizes are compatible) (Liu et al. 2020). The Ni-OEP molecules have an estimated surface area of 26.7 \AA^2 (PubChem 2019), presenting a twofold measurement of their approximate values dimensions ($\sim 5.17 \text{ \AA}$). Provided the materials' average pore diameters are larger than 20 \AA , it is possible to infer the diffusion of adsorbate molecules in the micropores of the adsorbents.

Due to the predominance of micropores on the CSAC porous surface, it was initially supposed that the use of activated carbon is associated with results of greater adsorption capacity results in comparison to the use of other materials.

Adsorbent selection

The q_e and $\%_{desorption}$ values obtained for each adsorbent material (CSAC, G and GO) employed in the initial Ni-OEP adsorption and desorption are shown in Table V. The values obtained were compared to the values observed in the literature for the use of other carbon-based materials, such as graphene and asphaltene.

As can be seen in Table V, the highest values of adsorption capacity are associated with the use of activated carbon ($5.73 \text{ mg}\cdot\text{g}^{-1}$). Compared to G and OG, this result may be associated with more favorable surface chemistry of CSAC, due to higher values of specific total area, pore distribution and presence of micropores. The closest values were obtained in similar works, in which graphene (Chen et al. 2018) and asphaltene (Chen et al. 2017) were used for the adsorption of Ni-OEP. The presence of different polarities of functional groups in asphaltene (Chen et al. 2017, 2018) and the greater interplanar distances in graphene (Wu et al. 2010), in relation to G and GO, may have been relevant characteristics for obtaining adsorption capacities close to $5 \text{ mg}\cdot\text{g}^{-1}$. Larger interplanar distances support the formation of larger porphyrin aggregates on the surface of the material, and may influence the selective adsorption of compounds (Kang et al. 2020). More functionalized surfaces can promote

the formation of more specific and intense adsorbent-adsorbent interactions during the adsorption process. The larger specific areas and volumes of micropores are associated with greater numbers of active sites available for adsorption. The higher content of oxygenated functional groups on the GO surface may have been a facilitator and limiting factor in the adsorption process, justifying the proximity of the adsorption capacity values in equilibrium with graphite. Acid-base interactions were potentially formed between the acid-character functionalized regions of GO and the basic-character nitrogenous regions of nickel porphyrins. However, these functional groups may have limited the access of Ni-OEP molecules to the interlayer space of the oxidized material (Feng et al. 2015), impairing the establishment of adsorbent-adsorbent interactions.

Despite the lower result of adsorption capacity, the use of graphite (G) is associated with a higher rate of Ni-OEP recovery with chloroform, reaching $\%_{desorption}$ values close to 50%. This performance may be related to the presence of less intense interactions between the non-functionalized graphitic surface and the metallic porphyrin, facilitating the desorption process. Due to the presence of acidic functional groups (carboxylics, epoxy and hydroxides) on the GO surface, intense interactions with the basic nitrogen regions of Ni-OEP, with chemisorption

or reactive adsorption characteristics as already reported for other aromatic compounds (Barroso-Bujans et al. 2010), may have hindered the desorption process. The tendency of porphyrinic molecules to form aggregates through π - π type stacks (Kumolo et al. 2019, Rytting et al. 2019), associated with high values of the CSAC specific area may be related to the significant desorption percentage obtained for the material, which was close to 31%. Chen et al. 2017, 2018 did not evaluate porphyrin recovery processes.

Considering the higher values of q_e and $\%_{desorption}$ obtained for CSAC, this material was chosen as adsorbent material in the subsequent experimental designs.

Experimental designs

Qualitative experimental design

The adsorption capacity and desorption percentage values obtained with the factorial type 2^2 design experiments are shown in Table VI.

According to the results obtained, we found that the change in the solvent used in the initial Ni-OEP solution did not cause significant changes in q_e , which ranged from 5.38 mg.g^{-1} , obtained with the use of toluene, to 5.07 mg.g^{-1} , obtained with the use of chloroform. Although the change of solvent (-1 to +1) caused a decrease in q_e of 0.28 mg.g^{-1} , there was no significant effect on the response variable. The differences observed in

Table VI. Qualitative design matrix and respective results of q_e , in mg.g^{-1} , and $\%_{desorption}$, in %, with adsorption initial solution of $8 \text{ }\mu\text{g.L}^{-1}$, at $T_{ads/des}$ of 298 K, $(S/L)_{ads}$ of 0.5 mg.mL^{-1} and $(S/L)_{des}$ of 0.2 mg.mL^{-1} , both under agitation of 120 rpm for 24 h.

Experiment	Solvent	Diluent	q_e (mg.g^{-1})	$\%_{desorption}$ (%)
1	-1	-1	5.36 ± 0.06	31.5 ± 0.8
2	+1	-1	5.07 ± 0.06	15.4 ± 0.7
3	-1	+1	5.38 ± 0.05	9.9 ± 0.1
4	+1	+1	5.11 ± 0.05	± 0.4

the experimental q_e might be a consequence of the greater porphyrin solubility in chloroform (Freeman et al. 1990). This provides a competitive medium for the adsorbent molecules, which have affinity with both the adsorbent active sites and the solvent molecules. This inverse relationship between solubility and the extent of adsorption capacity has been previously reported for the adsorption of aromatic compounds on activated carbon (Villacañas et al. 2006).

Regarding the desorptive processes outcomes, despite the greater solubility of porphyrin in dichloromethane in comparison to chloroform (Freeman et al. 1990), the %_{desorption} highest values were obtained using chloroform as diluent, reaching values close to 31%. The change of diluent (-1 to +1) led to a 14.2% decrease in %_{desorption}, indicating that the use of chloroform is more efficient in recovering porphyrin by desorption in relation to dichloromethane. The change of solvent (-1 to +1) led to a decrease of 8.7% in the %_{desorption}, which indicates that the use of toluene in the adsorption process favors a greater desorptive performance. The linear interaction between solvent and diluent led to a 7.4% increase in the %_{desorption}. Although the variables effects are more noticeable in the results of experimental %_{desorption}, these effects

were considered as little significant in the response variable during statistical analysis.

As the effects of the independent qualitative variables were little significant on the response variables, toluene and chloroform were selected as the most suitable solvent and diluent, respectively. The experimental results obtained and the possibility of working in a higher temperature range in subsequent procedures were considered for this decision.

Quantitative experimental design 2.1.10

The influence of the different temperature and solid/liquid ratio conditions employed in the adsorption process were evaluated through the statistical analysis of the experimental q_e results. They are shown in Supplementary Material - Table SI. The determined statistical parameters are presented in the form of ANOVA distribution in Table VII.

Considering the 90% as significance level and analyzing the F and p-values, we found that only $(S/L)_{ads}$ (x_2) in the linear form ($p < 0.10$) had a significant effect on q_e . The regression coefficients presented in Table VII show that $(S/L)_{ads}$ has a negative correlation with q_e . In other words, smaller $(S/L)_{ads}$ favor higher

Table VII. ANOVA parameters of quadratic polynomial regression model of q_e as a function of T_{ads} (x_1) and $(S/L)_{ads}$ (x_2).

Factor	Sum of Squares	Degree of freedom	Mean square	Regression coefficients	F-value	p-value
x_1	0.10	1	0.10	4.820	1.32	0.32
x_1^2	0.00	1	0.00	-0.124	0.01	0.94
x_2	13.45	1	13.45	-0.013	180.59	0.00*
x_2^2	0.12	1	0.12	-1.458	1.63	0.27
x_1x_2	0.07	1	0.07	0.212	0.91	0.39
Error	0.30	4	0.07			
Total	14.04	9				

*p-value < 0.10.

values of q_e due to the greater availability of adsorbent molecules (present in solution) in relation to the adsorbent active sites, promoting a greater likelihood of contact and formation of interactions. Similar results were achieved for the Ni-OEP and VO-OEP adsorption on asphaltene and graphene (Chen et al. 2013, 2017, 2018).

On the other hand, the adsorption temperature had no significant effect on q_e in the temperature range studied, in which we observed a behavior for the adsorption of heterocyclic nitrogen compounds on activated carbon (Wen et al. 2010). The evaluation of the temperature influence on adsorption can

be a complex process. While the increase in temperature can reduce the solution viscosity, facilitating the diffusion of the adsorbate molecules and increasing the adsorption rate (Yao et al. 2010), such variation can also promote an increase in the adsorbate solubility in the solvent, making competitive the affinity of the adsorbate for the solvent and the adsorbent surface. Favorable temperature conditions can be better analyzed through the thermodynamic study of the process (Lamichhane et al. 2016).

Quantitative experimental design 4.1.26

The $\%_{desorption}$ results obtained for the CCOD 4.1.26 adsorption and desorption experiments are

Table VIII. ANOVA parameters of quadratic polynomial regression model of $\%_{desorption}$ as a function of T_{ads} (x_1), $(S/L)_{ads}$ (x_2), T_{des} (x_3), and $(S/L)_{des}$ (x_4).

Factor	Sum of Squares	Degree of freedom	Mean square	Regression coefficients	F-value	p-value
x_1	11.81	1	11.81	18.161	2.35	0.15
x_1^2	22.75	1	22.75	0.761	4.53	0.06*
x_2	8.36	1	8.360	1.534	1.67	0.22
x_2^2	45.73	1	45.73	0.640	9.11	0.01*
x_3	583.68	1	583.68	2.175	116.31	0.00*
x_3^2	0.54	1	0.54	5.349	0.11	0.75
x_4	161.37	1	161.37	0.237	32.16	0.00*
x_4^2	14.91	1	14.91	-2.813	2.97	0.11
x_1x_2	9.17	1	9.17	1.242	1.83	0.20
x_1x_3	0.01	1	0.01	0.757	0.00	0.97
x_1x_4	5.97	1	5.97	-0.022	1.19	0.30
x_2x_3	40.15	1	40.15	-0.611	8.00	0.02*
x_2x_4	0.23	1	0.23	1.584	0.05	0.83
x_3x_4	3.10	1	3.10	-0.121	0.62	0.45
Error	55.20	11	5.02			
Total	962.98	25				

*p-value < 0.10.

presented in the matrix in Table SII. Percentages from 10.4 to 36.3% were obtained with the application of different temperature conditions and solid/liquid ratios for adsorption and desorption. The effects of the independent variables on the $\%_{desorption}$ were evaluated through the related statistical parameters presented in Table VIII.

Considering 90% as significance level, linear, quadratic and cross effects between the independent adsorption and desorption variables were verified in the $\%_{desorption}$. The variables referring to the desorption process had greater effects on $\%_{desorption}$: T_{des} (x_3), in the linear form, had the greatest effect due to its higher *F-value* (116.31), followed by $(S/L)_{des}$ (x_4), in the linear form, with *F-value* of 32.16. The adsorption variables had less significant effects on the desorption performance, as summarized in quadratic and cross interactions: $(S/L)_{ads}$ (x_2), in the quadratic form, presenting an effect similar to the interaction between $(S/L)_{ads}$ and T_{des} , with close *F-values* results (9.11 and 8, respectively), while T_{ads} (x_1), in the quadratic form, presented lesser effects. The other factors considered did not have any significant effect on the $\%_{desorption}$.

Concerning desorption conditions, whose effects on the desorption processes performance were superior to those from adsorption variables, it was possible to establish direct relationships with $\%_{desorption}$. In Table VIII, it was verified that T_{des} has a positive correlation and $(S/L)_{des}$ has a negative correlation with $\%_{desorption}$, through regression coefficients. In other words, higher T_{des} and lower $(S/L)_{des}$ favor higher values of the dependent variable. It is possible that the use of higher temperatures during the desorption process influenced the increase in the agitation degree of the solvent molecules, promoting a reduction in their viscosity as well as an increase in the diffusion rate on the surface of the adsorbent (Nasuha et al. 2010)

and adsorbate. This increases its energy level in relation to the adsorbed and solvated states, a necessary condition for the desorption of organic molecules (Ten Hulscher & Cornelissen 1996). The temperature can also be a key factor for the solubility increase of the porphyrinic molecules in the diluent, which increases the desorption rate. Meanwhile, the use of smaller amounts of adsorbent can facilitate the diluent-adsorbent contact, as a result of a greater availability of solvent molecules in the medium (Daneshvar et al. 2017).

As regards the adsorption variables, the same relationships cannot be directly established, in which the construction of response surfaces is required. It is discussed in detail in the optimization section.

Optimization

The order of relative relevance of the main effects of the independent variables, and the interactions of the variables with each other, in the evaluation variables can be observed in the Pareto charts (Saleh et al. 2018), shown in Figure 5. Considering a 90% significance level, the significant effects found were: $(S/L)_{ads}$ (x_2) in q_e (Figure 5a); and T_{des} (x_3), $(S/L)_{des}$ (x_4), quadratic interaction of $(S/L)_{ads}$ (x_2^2), interaction between $(S/L)_{ads}$ and T_{des} ($x_2 \cdot x_3$) and quadratic interaction of T_{ads} (x_1^2), in $\%_{desorption}$ (Figure 5b), in that order. Positive coefficients reveal positive contributions of the respective factors, while negative coefficients correspond to negative contributions. Factors whose effects did not reach the dashed line had no significant effect on the response variables.

The regression equation resulting of the dependent variable q_e as a function of the significant adsorption variables coded is presented in Equation 4, with R^2 close to 0.953.

$$q_e = 4.95 - 1.46x_2 \quad (4)$$

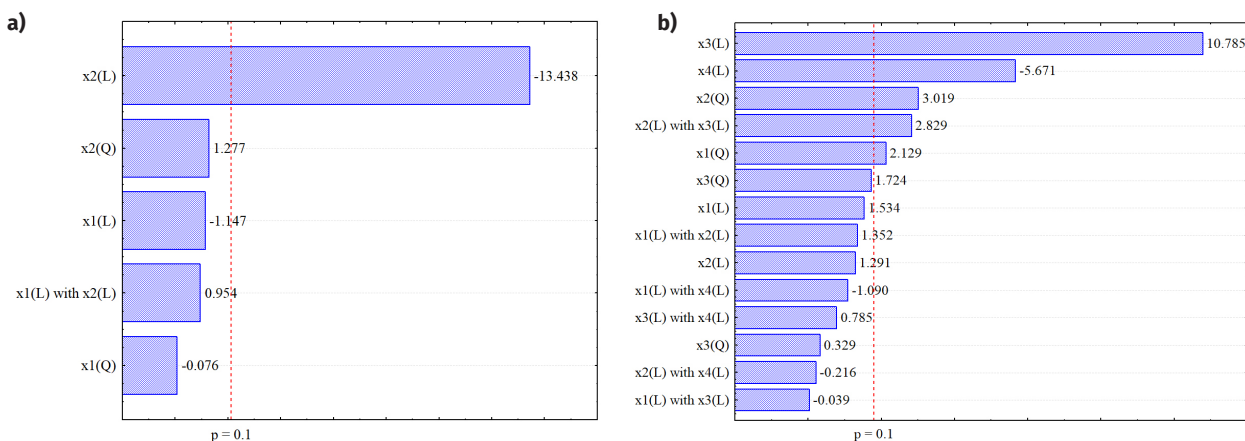


Figure 5. Pareto charts, at the 90% significance level, for (a) the coded adsorption variables (CCOD 2.1.10) and (b) the coded adsorption and desorption variables (CCOD 4.1.26).

The regression equation obtained for the $\%_{desorption}$ as a function of the significant variables is presented in Equation 5, with $R^2 = 0.871$.

$$\%_{desorption} = 18.4 + 1.5x_1^2 + 2.2x_2^2 + 5.4x_3 - 2.8x_4 + 1.6x_2x_3 \quad (5)$$

The adequacy of the adjustments is verified by the high determination coefficients of the regression equations obtained, close to the unit, and by the low residues between experimental and predicted values, illustrated in Figures S1 and S2.

The regression equations were used to simultaneously maximize the q_e and $\%_{desorption}$ values. The optimized conditions are shown in Table IX. They were consistent with the response surfaces behavior obtained for both response variables, as illustrated in Figures 6 and 7.

Within the pre-established conditions for the independent adsorption variables, it was possible to observe through the surface illustrated in Figure 6 that the smallest $(S/L)_{ads}$ resulted in the highest q_e values, for any T_{ads} value. The negative correlation between $(S/L)_{ads}$ and the evaluation variable q_e can be easily observed, keeping T_{ads} constant. The q_e results reached values close to 7 mg.g^{-1} , while the lowest

values reached 4 mg.g^{-1} for the largest $(S/L)_{ads}$. The T_{ads} did not significantly influence the q_e results, keeping $(S/L)_{ads}$ constant.

When evaluating the response surfaces obtained for $\%_{desorption}$ (Figure 7), we found that the use of T_{ads} and $(S/L)_{ads}$ upper and lower limits favored higher $\%_{desorption}$ values (Figure 7a). At the same time, higher T_{des} and smaller $(S/L)_{des}$ maximized this response variable (Figure 7b). Although it was not possible to establish a direct correlation between the adsorption variables in $\%_{desorption}$, positive correlation between T_{des} and $\%_{desorption}$ and negative correlation between $(S/L)_{des}$ were observed. The use of favorable conditions of $T_{ads/des}$ and $(S/L)_{ads/des}$ resulted in $\%_{desorption}$ experimental values close to 35%, whilst the unfavorable results reached 10%.

Thus, the optimal conditions were determined: lower T_{ads} (293 K), lower $(S/L)_{ads}$ (0.50 mg.mL^{-1}), higher T_{des} (323 K) and lower $(S/L)_{des}$ (0.20 mg.mL^{-1}), which resulted in the q_e and $\%_{desorption}$ maximized values of 6.91 mg.g^{-1} and 35.25%, respectively. The results in consonance with the information from the response surfaces were validated experimentally, in which a q_e close to 7.12 mg.g^{-1} e $\%_{desorption}$ of 37.7% were

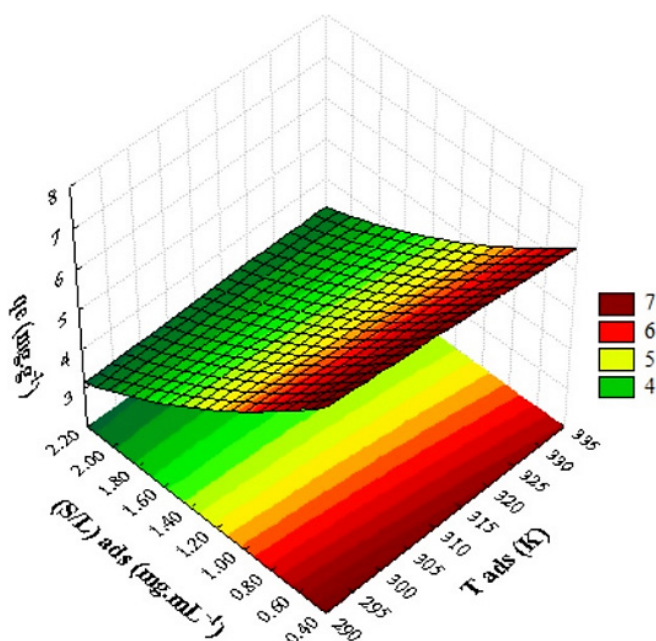


Figure 6. Response surface obtained for q_e (mg.g⁻¹), as a function of the adsorption variables, T_{ads} (294 to 332 K) and $(S/L)_{ads}$ (0.5 to 2.0 mg.mL⁻¹), with an initial solution of 8 $\mu\text{g.mL}^{-1}$, under agitation at 120 rpm for 24 h.

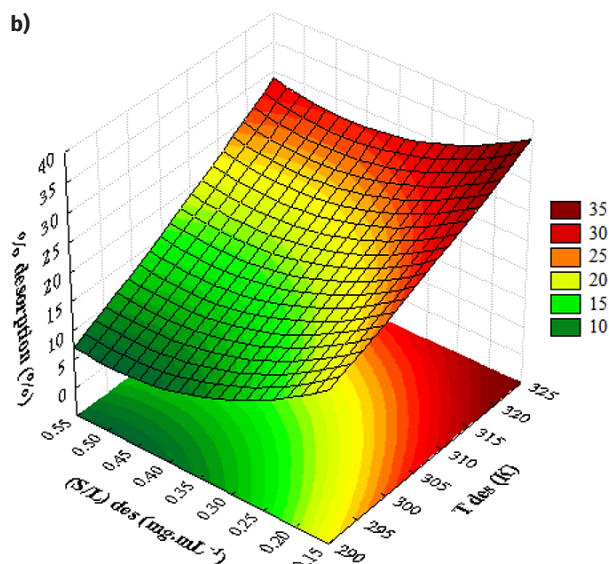
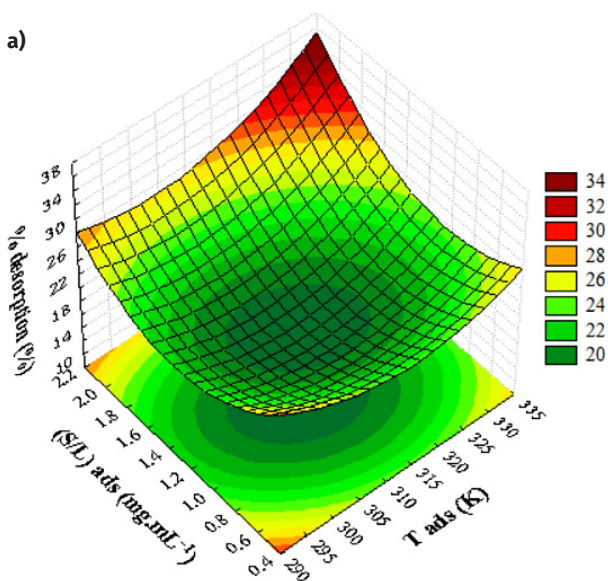


Figure 7. Response surface obtained for %_{desorption} (%) in (a) as a function of T_{ads} (294 to 332 K) and $(S/L)_{ads}$ (0.5 to 2.00 mg.mL⁻¹), and in (b) as a function of T_{des} (293 to 323 K) and $(S/L)_{des}$ (0.2 to 0.5 mg.mL⁻¹), with an initial solution of 8 $\mu\text{g.mL}^{-1}$ for adsorption, and both processes under agitation at 120 rpm for 24 h.

obtained. In relation to the results predicted, the deviations did not exceed 7%.

Since the experimental results are in agreement with those predicted by the optimized conditions, it was considered that the regression equations were adequate to describe

the processes behavior and to optimize the evaluation variables.

Ni-OEP desorption cycles

The adsorbent regeneration capacity is an important factor to be evaluated when studying

Table IX. Values of %_{removal}, q_e , %_{desorption} and q_{des} calculated for the respective Ni-OEP adsorption-desorption cycles in CSAC, under the optimized experimental conditions of adsorption and desorption.

Cycle	% _{removal} (%)	q_e (mg.g ⁻¹)	% _{desorption} (%)	q_{des} (mg.g ⁻¹)
1	61.76	9.88	29.04	2.87
2	51.34	8.22	34.99	2.87
3	11.42	1.83	182.04	3.33
4	10.04	1.61	276.19	4.44
5	6.98	1.12	357.03	3.99

the use of a specific material for the removal of contaminants, with both reuse and proper disposal purposes (Daneshvar et al. 2017).

The subsequent adsorption-desorption cycles of CSAC allowed the evaluation of this material in the removal and recovery of Ni-OEP, according to the results of %_{removal}, q_e , %_{desorption} and q_{des} presented in Table IX.

By means of the data shown in Table IX, there was a reduction in the removal percentage and adsorption capacity of Ni-OEP on CSAC (%_{removal} and q_e , respectively), with an increase in the number of cycles. The most significant difference was observed after the second cycle, with a reduction of approximately 78% of %_{removal} and q_e values (%_{removal,3 cycle}rd = 0.22%_{removal,2 cycle}nd and $q_{e,3 cycle}$ rd = 0.22 $q_{e,2 cycle}$ nd).

Despite the decrease in the variables associated with the adsorption of Ni-OEP on the CSAC surface, an increase in the porphyrin desorption percentage and capacity (%_{desorption} and q_{des} , respectively) was observed from each cycle, gradually. Therefore, there was the desorption of Ni-OEP molecules adsorbed in previous cycles, which provides a proper rationale for the %_{desorption} values above 100% from the 3rd cycle onwards. Probably, as the cycles progressed, the intensity of the adsorbent-adsorbent interactions decreased, favoring desorption. This effect,

known as the carry-over effect, is a recurring problem in HPLC (High-Performance Liquid Chromatography) analyzes due to interference in quantitative results per run (Mitulovic et al. 2009). However, the results obtained at the end of the regeneration cycles showed that the carry-over effects are favorable to the increase of the partial results obtained per cycle.

Considering the five cycles, 22.66 mg.g⁻¹ of Ni-OEP were adsorbed, wherein approximately 77% (17.5 mg.g⁻¹) of the adsorbed porphyrins were recovered. In similar studies, nickel is reasonably removed from adsorbent materials using elution systems composed of hydrochloric acid solution (Shahat et al. 2018, Xu et al. 2018). However, the acid-base elution was not considered in the present study due to the recovery of only the metal ion, keeping the free base porphyrin, which is of commercial interest, still adsorbed on the material.

Probable adsorption mechanisms

The knowledge of the possible mechanisms involved in the adsorption of Ni-OEP on CSAC can be facilitated with the assimilation of the interactions established between the porphyrinic molecules and the other constituents of the oil asphaltic fraction or the organic fraction of the bituminous shales. Some authors suggest

the fundamental role of petroporphyrins in the asphaltene aggregation mechanisms (Borisova et al. 2017, Gawrys et al. 2006, Munoz et al. 2019, Santos Silva et al. 2018), whose predominant interactions are distributed between van der Waals dispersion, electrostatic, multipolar, hydrogen bonds and repulsive steric interactions (Castillo & Vargas 2016, Rytting et al. 2019). With a tetrapyrrolic base structure, the porphyrins found in the oil are defined by the nature of their metallic center and lateral substituting groups. The structural and electronic configurations of the petroporphyrinic molecules interfere in the interactions established with other components and in their self-association connections, enabling the formation of π - π type stacks, metal-metal interactions, metal-substituting group or dipole-dipole between peripheral substituting groups (Fan et al. 2020, Jentzen et al. 2016).

Considering the aromatic base structure formed by sp^2 hybridization carbons, which is common to all adsorbents used, it is likely that dispersive interactions of the type π - π have been established not only between metalloporphyrinic molecules but between Ni-OEP molecules and the CSAC basic structure. In addition, the polar functional groups present on the surface of activated carbon may have favored the formation of a greater intensity adsorbent-adsorbent interactions of the dipole-dipole or acid-base type.

Dispersive acid-base interactions are likely to be identified between acidic oxygenated functional groups present on the surface of the CSAC and the basic nitrogenous regions of the porphyrin rings (Lee et al. 2017). Some authors highlight the importance of carboxylic groups in the establishment of interactions with nitrogen compounds, improving the adsorption performance of these components on activated carbon (Almarri et al. 2009, Na et al. 2011). Dispersive interactions are also potentially

established between the metallic center of porphyrin, which is acidic (Lee et al. 2017) and reactive (Gottfried 2015), and functional groups of basic character on the surface of the CSAC, identified in a similar proportion to the acid groups, according to the characterization performed by Ferreira et al. 2019.

The less energetic interactions, established during the formation of multiporphyrinic aggregates on the surface of the CSAC, were more easily broken during the desorption process with chloroform. However, the more intense interactions, characteristic of the formation of porphyrinic occlusions and reactive adsorption, were the greatest obstacles to desorption (Castillo & Vargas 2016, Derakhshesh et al. 2013). Part of the remaining amount of porphyrin on the activated carbon surface can be in the form of tectons, constituents of adlayers formed during the adsorption of octaethylporphyrins on graphitic based surfaces (Hippis & Mazur 2018, Ogunrinde et al. 2006). The initially lower values of $\%_{desorption}$ may be associated with the difficulty of breaking the most energetic interactions, which is partially reduced by the application of higher T_{des} values and the successive adsorption cycles. The separation of petroporphyrin compounds can be facilitated by preventing the formation of occlusions (Fan et al. 2020).

In addition, the significative recovery of adsorbed and adsorbent materials allows the evolution of separation methods aiming the environmental and financial sustainability of the process. The recovered porphyrins can be used as an alternative to their synthetic counterparts in the catalytic area, while the activated carbon can be reused in new adsorption-desorption cycles. The low rate of waste generation as well as the reuse of materials and minimization of input consumption are pillars of the circular economy (Henckens et al. 2016, Londoño & Cabezas 2021).

CONCLUSIONS

The performance of Ni-OEP adsorption tests on different adsorbents and the execution of the qualitative and quantitative experimental plans allowed the selection of conditions that favor the highest q_e and $\%_{desorption}$ values. The most efficient adsorbent in removing metalloporphyrin from an initial solution with toluene was CSAC. The likely rationale for this outcome is due to the combination of its favorable surface characteristics: greater functionalization, developed micropore structure and higher values of specific surface area and pore volume. It is possible that the fraction of the adsorbed porphyrin was desorbed due to the establishment of less intense π - π type adsorbate-adsorbate interactions, whereas the more intense adsorbate-adsorbent interactions occurred by virtue of acid-base reactive adsorption characteristics, keeping part of the molecules of Ni-OEP still in the adsorbed state.

The conditions for simultaneous maximization of the evaluation variables (q_e and $\%_{desorption}$) were: toluene as a solvent, chloroform as a diluent, lowest T_{ads} (293 K), lowest $(S/L)_{ads}$ (0.5 mg.mL⁻¹), lowest $(S/L)_{des}$ (0.2 mg.mL⁻¹) and greatest T_{des} (323 K), considering the pre-established conditions. The regression equations obtained, and the optimization results were adequate to the adsorption and desorption experimental data of the Ni-OEP behavior.

The results of optimized adsorption capacity and desorption percentage were reproduced in the first adsorption-desorption cycles, indicating the reproducibility of the processes under optimal conditions. At the end of the 5 cycles, approximately 77% of the Ni-OEP adsorbed on CSAC were recovered. The results obtained show the potential of study of carbon-based materials and experimental conditions in the recovery of porphyrin compounds from

real oils and bituminous shales. Materials with structures similar to asphaltenic components could be interesting due to the possibility of formation of porphyrinic aggregates by π - π interaction and consequent facility of recovery of the materials.

Acknowledgments

This study was financed by the Coordenação de Aperfeiçoamento de Pessoal de Nível Superior – Brasil (CAPES) – Finance Code 001. The authors would like to acknowledge CAPES for financial support; the Multiuser Laboratory of Pontal at the Federal University of Uberlândia (FINEP/2013 INFR13 01.13.0371.00) and Multiuser Analysis Center from IQ-UFG for the technical and scientific support; and Bahiacarbon Agro-industrial (Bahia, Brazil) for the samples of activated carbon granted.

REFERENCES

- AFFOURI H & SAHRAOUI O. 2017. The sedimentary organic matter from a Lake Ichkeul core (far northern Tunisia): Rock-Eval and biomarker approach. *J African Earth Sci* 129: 248-259.
- ALMARRI M, MA X & SONG C. 2009. Selective adsorption for removal of nitrogen compounds from liquid hydrocarbon streams over carbon-and alumina-based adsorbents. *Ind Eng Chem Res* 48(2): 951-960.
- ASGAR H, DEEN KM, RIAZ U, RAHMAN ZU, SHAH UH & HAIDER W. 2018. Synthesis of graphene via ultra-sonic exfoliation of graphite oxide and its electrochemical characterization. *Mater Chem Phys* 206: 7-11.
- BARRETT EP, JOYNER LG & HALENDA PP. 1951. The determination of pore volume and area distributions in porous substances. I. Computations from nitrogen isotherms. *J Am Chem Soc* 73(1): 373-380.
- BARROSO-BUJANS F, CERVENY S, ALEGRÍA A & COLMENERO J. 2010. Sorption and desorption behavior of water and organic solvents from graphite oxide. *Carbon* 48(11): 3277-3286.
- BIN-DAHMAN OA & SALEH TA. 2020. Synthesis of carbon nanotubes grafted with PEG and its efficiency for the removal of phenol from industrial wastewater. *Environ Nanotechnol Monit Manag* 13: 100286.
- BORISOVA YY, TAZEEVA EG, MIRONOV NA, BORISOV DN, YAKUBOVA SG, AILOVA GR, SINYASHIN KO & YAKUBOV MR.

2017. Role of vanadylporphyrins in the flocculation and sedimentation of asphaltenes of heavy oils with high vanadium content. *Energy Fuels* 31(12): 13382-13391.
- BRUNAUER S, EMMETT PH & TELLER E. 1938. Adsorption of gases in multimolecular layers. *J Am Chem Soc* 60(2): 309-319.
- CARVALHO MAFD, AGUIAR DV, AGUIAR A, VAZ BG, FERREIRA MEDO, ANDRADE LDA & OSTROSKI IC. 2020. A potential material for removal of nitrogen compounds in petroleum and petrochemical derivatives. *Chem Eng Commun* 1-16.
- CASTILLO J & VARGAS V. 2016. Metal porphyrin occlusion: Adsorption during asphaltene aggregation. *Pet Sci Technol* 34(10): 873-879.
- CHANNEI D, NAKARUK A & PHANICHPHANT S. 2018. Controlled oxidative ageing time of graphite/graphite oxide to graphene oxide in aqueous media. *J Aust Ceram Soc* 54(1): 91-96.
- CHEN F, LIU Q, ZU Z, SUN X, SHI Q & ZHAO S. 2013. Adsorption kinetics and thermodynamics of vanadyl etioporphyrin on asphaltene in pentane. *Energy Fuels* 27(11): 6408-6418.
- CHEN F, ZHU Q, LI S, XU Z, SUN X & ZHAO S. 2018. The function of poly aromatic nuclei structure for adsorption of vanadyl/nickel etioporphyrin on asphaltene/graphene. *Fuel Process Technol* 174: 132-141.
- CHEN F, ZHU Q, XU Z, SUN X & ZHAO S. 2017. Metal porphyrin adsorption onto asphaltene in pentane solution: a comparison between vanadyl and nickel etioporphyrins. *Energy Fuels* 31(4): 3592-3601.
- DANESHVAR E, VAZIRZADEH A, NIAZI A, KOUSHA M, NAUSHAD M & BHATNAGAR A. 2017. Desorption of methylene blue dye from brown macroalga: effects of operating parameters, isotherm study and kinetic modeling. *J Clean Prod* 152: 443-453.
- DECHAINE GP & GRAY MR. 2010. Chemistry and association of vanadium compounds in heavy oil and bitumen, and implications for their selective removal. *Energy Fuels* 24(5): 2795-2808.
- DEMIRBAS A, BAFAIL A & NIZAMI A. 2016. Heavy oil upgrading: Unlocking the future fuel supply. *Pet Sci Technol* 34(4): 303-308.
- DERAKHSHESH M, BERGMANN A & GRAY MR. 2013. Occlusion of polyaromatic compounds in asphaltene precipitates suggests porous nanoaggregates. *Energy Fuels* 27(4): 1748-1751.
- ETIM UJ, WU P, BAI P, XING W, ULLAH R, SUBHAN F & YAN Z. 2016. Location and Surface Species of Fluid Catalytic Cracking Catalyst Contaminants: Implications for Alleviating Catalyst Deactivation. *Energy Fuels* 30(12): 10371-10382.
- ETIM UJ, BAI P, LIU X, SUBHAN F & ULLAH R. 2019. Vanadium and nickel deposition on FCC catalyst: Influence of residual catalyst acidity on catalytic products. *Microporous Mesoporous Mater* 273: 276-285.
- FAN S, LIU H, WANG J, CHEN H, BAI R, GUO A, CHEN K, HUANG J & WANG Z. 2020. Microwave-assisted Petroporphyrin Release from Asphaltene Aggregates in Polar Solvents. *Energy Fuels* 34(3): 2683-2692.
- FENG X, MAX, LI N, SHANG C, YANG X & CHEN XD. 2015. Adsorption of quinoline from liquid hydrocarbons on graphite oxide and activated carbons. *RSC Adv* 5(91): 74684-74691.
- FERREIRA MEO, VAZ BG, BORBA CE, ALONSO CG & OSTROSKI IC. 2019. Modified activated carbon as a promising adsorbent for quinoline removal. *Microporous Mesoporous Mater* 277: 208-216.
- FREEMAN DH, SWAHN ID & HAMBRIGHT P. 1990. Spectrophotometry and solubility properties of nickel and vanadyl porphyrin complexes. *Energy Fuels* 4(6): 699-704.
- GAWRYS KL, BLANKENSHIP GA & KILPATRICK PK. 2006. On the distribution of chemical properties and aggregation of solubility fractions in asphaltenes. *Energy Fuels* 20(2): 705-714.
- GOTTFRIED JM. 2015. Surface chemistry of porphyrins and phthalocyanines. *Surf Sci Rep* 70(3): 259-379.
- GRUDEN-PAVLOVIĆ M, GRUBIŠIĆ S, ZLATAR M & NIKETIĆ SR. 2007. Molecular mechanics study of nickel (II) octaethylporphyrin adsorbed on graphite (0001). *Int J Mol Sci* 8(8): 810-829.
- HAN X, LIN H & ZHENG Y. 2015. The role of oxygen functional groups in the adsorption of heteroaromatic nitrogen compounds. *J Hazard Mater* 297: 217-223.
- HENCKENS MLCM, DRIESSEN PPJ, RYNGAERT C & WORRELL E. 2016. The set-up of an international agreement on the conservation and sustainable use of geologically scarce mineral resources. *Resour Policy* 49: 92-101.
- HIPPS KW & MAZUR U. 2018. Kinetic and thermodynamic control in porphyrin and phthalocyanine self-assembled monolayers. *Langmuir* 34(1): 3-17.
- JENTZEN W, SHELNUTT JA & SCHEIDT WR. 2016. Metalloporphines: dimers and trimers. *Inorg Chem* 55(12): 6294-6299.
- JUROW M, SCHUCKMAN AE, BATTEAS JD & DRAIN CM. 2010. Porphyrins as molecular electronic components of functional devices. *Coord Chem Rev* 254(19-20): 2297-2310.
- KANG JY, HA W, ZHANG HX & SHI YP. 2020. Sodium (I)-doped graphitic carbon nitride with appropriate interlayer

distance as a highly selective sorbent for strontium (II) prior to its determination by ICP-OES. *Microchim Acta* 187(1): 1-9.

KHAN H, YERRAMILI AS, D'OLIVEIRA A, ALFORD TL, BOFFITO DC & PATIENCE GS. 2020. Experimental methods in chemical engineering: X-ray diffraction spectroscopy—XRD. *Can J Chem Eng* 98(6): 1255-1266.

KORIAKIN A, PONVEL KM & LEE C. 2010. Denitrogenation of raw diesel fuel by lithium-modified mesoporous silica. *Chem Eng J* 162(2): 649-655.

KUMOLO ST, YULIZAR Y, HAERUDIN H, KURNIAWATY I & APRIANDANU DOB. 2019. Identification of metal porphyrins in Duri crude oil. In: *IOP Conference Series: Materials Science and Engineering* 496(1): 012038.

KUZMIN SM, CHULOZSKAYA SA & PARFENYUK VI. 2018. Structures and properties of porphyrin-based film materials part I. The films obtained via vapor-assisted methods. *Adv Colloid Interface Sci* 253: 23-34.

LAMICHHANE S, KRISHNA KCB & SARUKKALIGE R. 2016. Polycyclic aromatic hydrocarbons (PAHs) removal by sorption: a review. *Chemosphere* 148: 336-353.

LEE H, HONG K & JANG W. 2017. Design and applications of molecular probes containing porphyrin derivatives. *Coord Chem Rev* 354: 46-73.

LI Y, SHANG H, ZHANG Q, ELABYOUKI M & ZHANG W. 2020. Theoretical study of the structure and properties of Ni/V porphyrins under microwave electric field: A DFT study. *Fuel* 278: 118305.

LIPPENS BC & DE BOER JH. 1965. Studies on pore systems in catalysts: V. The t method. *J Catal* 4(3): 319-323.

LIU H, LIN C, WANG Z, GUO A & CHEN K. 2015a. Ni, V, and porphyrinic V distribution and its role in aggregation of asphaltenes. *J Dispers Sci Technol* 36(8): 1140-1146.

LIU H, LONG L, WENG X, ZHENG S & XU Z. 2020. Efficient removal of tetrabromobisphenol A using microporous and mesoporous carbons: the role of pore structure. *Microporous Mesoporous Mater* 298: 110052.

LIU H, WANG Z, GUO A, LIN C & CHEN K. 2015b. The distribution of Ni and V in resin and asphaltene subfractions and its variation during thermal processes. *Pet Sci Technol* 33(2): 203-210.

LONDOÑO NAC & CABEZAS H. 2021. Perspectives on circular economy in the context of chemical engineering and sustainable development. *Cur Opin Chem Eng* 34: 100738.

MARCANO DC, KOSYNKIN DV, BERLIN JM, SINITSKII A, SUN Z, SLESAREV A, ALEMANY LB, LU W & TOUR JM. 2010. Improved synthesis of graphene oxide. *ACS Nano* 4(8): 4806-4814.

MARLER RT & ARORA JS. 2010. The weighted sum method for multi-objective optimization: new insights. *Struct Multidiscip Optim* 41(6): 853-862.

MIRONOV NA, SINYASHIN KO, ABILOVA GR, TAZEVA EG, MILORDOV DV, YAKUBOVA SG, BORISOV DN, GRYAZNOV PI, BORISOVA YY & YAKUBOV MR. 2017. Chromatographic isolation of vanadyl porphyrins from heavy oil resins. *Russ Chem Bull* 66(8): 1450-1455.

MIRONOV NA, ABILOVA GR, BORISOVA YY, TAZEVA EG, MILORDOV DV, YAKUBOVA SG & YAKUBOV MR. 2018a. Comparative Study of Resins and Asphaltenes of Heavy Oils as Sources for Obtaining Pure Vanadyl Porphyrins by the Sulfocationite-Based Chromatographic Method. *Energy Fuels* 32(12): 12435-12446.

MIRONOV NA, ABILOVA GR, SINYASHIN KO, GRYAZNOV PI, BORISOVA YY, MILORDOV DV, TAZEVA EG, YAKUBOVA SG, BORISOV DN & YAKUBOV MR. 2018b. Chromatographic isolation of petroleum vanadyl porphyrins using sulfocationites as sorbents. *Energy Fuels* 32(1): 161-168.

MITULOVIC G, STINGL C, STEINMACHER I, HUDECZ O, HUTCHINS JR, PETERS JM & MECHTLER K. 2009. Preventing carryover of peptides and proteins in nano LC-MS separations. *Anal Chem* 81(14): 5955-5960.

MOSKVIN LN. 2016. A classification of separation methods. *Sep Purif Rev* 45(1): 1-27.

MOUSAVI M, HOSSEINNEZHAD S, HUNG AM & FINI EH. 2019. Preferential adsorption of nickel porphyrin to resin to increase asphaltene precipitation. *Fuel* 236: 468-479.

MUNOZ G, GUNESSE BK, BÉGUÉ D, BOUYSSIERE B, BARAILLE I, VALLVERDU G & SILVA HS. 2019. Redox activity of nickel and vanadium porphyrins: a possible mechanism behind petroleum genesis and maturation? *RSC Adv* 9(17): 9509-9516.

NA LI, ALMARRI M & ZHA QF. 2011. The role of surface oxygen-containing functional groups in liquid-phase adsorptive denitrogenation by activated carbon. *New Carbon Mater* 26(6): 470-478.

NASUHA N, HAMEED BH & DIN ATM. 2010. Rejected tea as a potential low-cost adsorbent for the removal of methylene blue. *J Hazard Mater* 175(1-3): 126-132.

OGUNRINDE A, HIPPS KW & SCUDIERO L. 2006. A scanning tunneling microscopy study of self-assembled nickel (II) octaethylporphyrin deposited from solutions on HOPG. *Langmuir* 22(13): 5697-5701.

POIRIER L, NELSON J, LEONG D, BERHANE L, HAJDU P & LOPEZ-LINARES F. 2016. Application of ICP-MS and ICP-OES on the determination of nickel, vanadium, iron, and calcium in

- petroleum crude oils via direct dilution. *Energy Fuels* 30(5): 3783-3790.
- PRADO GHC, RAO Y & DE KLERK A. 2016. Nitrogen removal from oil: a review. *Energy Fuels* 31(1): 14-36.
- PUBCHEM. 2019. Compound Summary: 2,3,7,8,12,13,17,18-Octaethyl-21H,23H-porphine nickel(II). National Center for Biotechnology Information. Bethesda: National Library of Medicine. <https://pubchem.ncbi.nlm.nih.gov/compound/526506#section=Computed-Properties>.
- RAMÍREZ-PRADILLA JS, BLANCO-TIRADO C, HUBERT-ROUX M, GIUSTI P, AFONSO C & COMBARIZA MY. 2019. Comprehensive petroporphyrin identification in crude oils using highly selective electron transfer reactions in MALDI-FTICR-MS. *Energy Fuels* 33(5): 3899-3907.
- REGTI A, LAAMARI MR, STIRIBA SE & EL HADDAD M. 2017. Use of response factorial design for process optimization of basic dye adsorption onto activated carbon derived from *Persea* species. *Microchem J* 130: 129-136.
- RIBEIRO JN, SILVA RA, PELEGRINI A, TEDESCO AC & JORGE RA. 2005. Evaluation of photodynamic activity of octaethylporphyrin and vanadyl octaethylporphyrin. *Appl Cancer Res* 25(3): 142-150.
- RYTTING BM, SINGH ID, KILPATRICK PK, HARPER MR, MENNITO AS & ZHANG Y. 2018. Ultrahigh-purity vanadyl petroporphyrins. *Energy Fuels* 32(5): 5711-5724.
- RYTTING BM, HARPER MR, EDMOND KV, ZHANG Y & KILPATRICK PK. 2019. High-Purity Vanadyl Petroporphyrins: Their Aggregation and Effect on the Aggregation of Asphaltenes. *Energy Fuels* 34(1): 164-178.
- SALEH TA. 2011. The influence of treatment temperature on the acidity of MWCNT oxidized by HNO₃ or a mixture of HNO₃/H₂SO₄. *Appl Surf Sci* 257(17): 7746-7751.
- SALEH TA. 2020. Characterization, determination and elimination technologies for sulfur from petroleum: Toward cleaner fuel and a safe environment. *Trends Environ Anal Chem* 25: e00080.
- SALEH TA, ADIO SO, ASIF M & DAFALLA H. 2018. Statistical analysis of phenols adsorption on diethylenetriamine-modified activated carbon. *J Clean Prod* 182: 960-968.
- SALEH TA, ELSHARIF AM, ASIRI S, MOHAMMED ARI & DAFALLA H. 2020. Synthesis of carbon nanotubes grafted with copolymer of acrylic acid and acrylamide for phenol removal. *Environ Nanotechnol Monit Manag* 14: 100302.
- SAMA SG, BARRÈRE-MANGOTE C, BOUYSSIÈRE B, GIUSTI P & LOBINSKI R. 2018. Recent trends in element speciation analysis of crude oils and heavy petroleum fractions. *Trends Analyt Chem* 104: 69-76.
- SANO Y, CHOI KH, KORAI Y & MOCHIDA I. 2004. Effects of nitrogen and refractory sulfur species removal on the deep HDS of gas oil. *Appl Catal B* 53(3): 169-174.
- SANTOS SILVA H, ALFARRA A, VALLVERDU G, BÉGUÉ D, BOUYSSIÈRE B & BARAILLE I. 2018. Impact of H-bonds and porphyrins on asphaltene aggregation as revealed by molecular dynamics simulations. *Energy Fuels* 32(11): 11153-11164.
- SHAH SS, AHMAD I, AHMAD W, ISHAQ M & KHAN H. 2017. Deep desulphurization study of liquid fuels using acid treated activated charcoal as adsorbent. *Energy Fuels* 31(8): 7867- 7873.
- SHAHAT A, HASSAN HM, EL-SHAHAT MF, EL SHAHAWY O & AWUAL MR. 2018. Visual nickel (II) ions treatment in petroleum samples using a mesoporous composite adsorbent. *Chem Eng J* 334: 957-967.
- SIGMA ALDRICH. 2021. Sigma Aldrich Product Catalog. 2021. Available in: <https://www.sigmaaldrich.com/catalog/product/aldrich/269948?lang=ptregion=BR>. Acess on May 28, 2021.
- SILVA NK, SILVA DO, VIEIRA LG & BARROZO MA. 2015. Effects of underflow diameter and vortex finder length on the performance of a newly designed filtering hydrocyclone. *Powder Technol* 286: 305-310.
- SILVA HS, SODERO ACR, KORB JP, ALFARRA A, GIUSTI P, VALLVERDU G, BÉGUÉ D, BARAILLE I & BOUYSSIÈRE B. 2017. The role of metalloporphyrins on the physical-chemical properties of petroleum fluids. *Fuel* 188: 374-381.
- SOROKINA TP, BULUCHEVSKAYA LA, POTAPENKO OV & DORONIN VP. 2010. Conversion of nickel and vanadium porphyrins under catalytic cracking conditions. *Pet Chem* 50(1): 51-55.
- STORN R & PRICE K. 1997. Differential evolution - A simple and efficient adaptive scheme for global optimization over continuous spaces. *J Glob Optim* 11(4): 341-359.
- SUGIYAMA I & WILLIAMS-JONES AE. 2018. An approach to determining nickel, vanadium and other metal concentrations in crude oil. *Anal Chim Acta* 1002: 18-25.
- TEN HULSCHER TEM & CORNELISSEN G. 1996. Effect of temperature on sorption equilibrium and sorption kinetics of organic micropollutants-a review. *Chemosphere* 32(4): 609-626.
- THOMMES M, KANEKO K, NEIMARK AV, OLIVIER JP, RODRIGUEZ-REINOSO F, ROUQUEROL J & SING KS. 2015. Physisorption of gases, with special reference to the evaluation of surface

area and pore size distribution (IUPAC Technical Report). *Pure Appl Chem* 87(9-10): 1051-1069.

VILLACAÑAS F, PEREIRA MFR, ÓRFÃO JJ & FIGUEIREDO JL. 2006. Adsorption of simple aromatic compounds on activated carbons. *J Colloid Interface Sci* 293(1): 128-136.

WANG B, KURIAN V, MAHAPATRA N, MARTENS F & GUPTA R. 2016. Investigation of corrosion and fouling in syngas cooler tubes. *Fuel Process Technol* 141: 202-209.

WEN J, HAN X, LIN H, ZHENG Y & CHU W. 2010. A critical study on the adsorption of heterocyclic sulfur and nitrogen compounds by activated carbon: equilibrium, kinetics and thermodynamics. *Chem Eng J* 164(1): 29-36.

WEN J, LIN H, HAN X, ZHENG Y & CHU W. 2017. Physicochemical studies of adsorptive denitrogenation by oxidized activated carbons. *Ind Eng Chem Res* 56(17): 5033-5041.

WOLTERING M, TULIPANI S, BOREHAM CJ, WALSHE J, SCHWARK L & GRICE K. 2016. Simultaneous quantitative analysis of Ni, VO, Cu, Zn and Mn geoporphyrins by liquid chromatography-high resolution multistage mass spectrometry: Method development and validation. *Chem Geol* 441: 81-91.

WU Y, WANG B, MA Y, HUANG Y, LI N, ZHANG F & CHEN Y. 2010. Efficient and large-scale synthesis of few-layered graphene using an arc-discharge method and conductivity studies of the resulting films. *Nano Res* 3(9): 661-669.

XU J, CHEN L, GENG T, REN M, WANG S, SONG Z & CAO F. 2018. Spherical polymer brushes bearing imidazole groups as novel nickel remover for crude oil. *Fuel* 226: 47-53.

YAKUBOV MR, ABILOVA GR, SINYASHIN KO, MILORDOV DV, TAZEVA EG, YAKUBOVA SG, BORISOV DN, GRYAZNOV PI, MIRONOV NA & BORISOVA YY. 2017. Isolation of porphyrins from heavy oil objects. *Phthalocyanines and Some Current Applications* 153-168.

YANG W, GAO Y & CASEY JF. 2018. Determination of trace elements in crude oils and fuel oils: A comprehensive review and new data. In *Solution chemistry: Advances in research and applications*, 159-205. New York: Nova Science Publishers Hauppauge.

YAO Y, XU F, CHEN M, XU Z & ZHU Z. 2010. Adsorption behavior of methylene blue on carbon nanotubes. *Bioresour Technol* 101(9): 3040-3046.

ZHANG Y ET AL. 2019. Elucidating the Geometric Substitution of Petroporphyrins by Spectroscopic Analysis and Atomic Force Microscopy Molecular Imaging. *Energy Fuels* 33(7): 6088-6097.

ZHAO X, XU C & SHI Q. 2015. Porphyrins in Heavy Petroleum: A Review. In *Structure and Modeling of Complex Petroleum Mixtures*, 39-70. Cham: Springer.

ZHAO Y, CHO CW, CUI L, WEI W, CAI J, WU G & YUN YS. 2019. Adsorptive removal of endocrine-disrupting compounds and a pharmaceutical using activated charcoal from aqueous solution: kinetics, equilibrium, and mechanism studies. *Environ Sci Pollut Res* 26(33): 33897-33905.

How to cite

CAETANO GC, ANDRADE LA, MARTINS PR & OSTROSKI IC. 2023. Optimization of the adsorption and desorption processes of nickel octaethylporphyrin in carbon-based adsorbents. *An Acad Bras Cienc* 95: e20190676. DOI 10.1590/0001-376520230211598.

SUPPLEMENTARY MATERIAL

Tables SI-SII.

Figures S1-S2.

Manuscript received on December 15, 2021; accepted for publication on June 14, 2022

GABRIELA COSTA CAETANO¹

<https://orcid.org/0000-0002-4817-7003>

LAIANE ALVES DE ANDRADE²

<https://orcid.org/0000-0003-0012-4575>

PAULO ROBERTO MARTINS¹

<https://orcid.org/0000-0002-3227-0190>

INDIANARA CONCEIÇÃO OSTROSKI¹

<https://orcid.org/0000-0002-9265-7143>

¹Federal University of Goiás, Institute of Chemistry, Av. Esperança, s/n, 74690-900 Goiânia, GO, Brazil

²Federal University of Mato Grosso do Sul, Department of Production Engineering, Av. Antônio Joaquim de Moura Andrade, 2310, 79750-000 Nova Andradina, MS, Brazil

Correspondence to: **Indianara Conceição Ostroski**

E-mail: indianara_ostroski@ufg.br

Author contributions

Gabriela Costa Caetano: Methodology, Validation, Investigation, Data Curation, Writing - Original Draft, Visualization. Laiane Alves de Andrade: Software, Formal analysis. Paulo Roberto Martins: Methodology, Resources. Indianara Conceição Ostroski: Conceptualization, Methodology, Resources, Writing - Review Editing, Supervision, Project administration, Funding acquisition.

